THE ROYAL SOCIETY

Received 8 January 2003
Accepted 26 March 2003
Published online 12 June 2003

Transients and attractors in epidemics

Chris T. Bauch* **and David J. D. Earn**

Department of Mathematics and Statistics, McMaster University, Hamilton, Ontario L8S 4K1, Canada

Historical records of childhood disease incidence reveal complex dynamics. For measles, a simple model has indicated that epidemic patterns represent attractors of a nonlinear dynamic system and that transitions between different attractors are driven by slow changes in birth rates and vaccination levels. The same analysis can explain the main features of chickenpox dynamics, but fails for rubella and whooping cough. We show that an additional (perturbative) analysis of the model, together with knowledge of the population size in question, can account for all the observed incidence patterns by predicting how stochastically sustained transient dynamics should be manifested in these systems.

Keywords: childhood disease dynamics; seasonal forcing; SEIR model; perturbation theory; demographic stochasticity; Poincaré map

1. INTRODUCTION

Understanding the complex incidence patterns of childhood diseases during the twentieth century has been a major goal of mathematical epidemiology (London & Yorke 1973; Dietz 1975; Schaffer 1985; Anderson & May 1991; Grenfell 1992; Earn *et al.* 1998, 2000; Rohani *et al.* 1999). Case notifications going back to the early twentieth century show a variety of outbreak patterns, including regular cycles of various lengths and apparently aperiodic dynamics (Bartlett 1957; Yorke & London 1973; Olsen & Schaffer 1990; Bolker & Grenfell 1993); moreover, the temporal epidemic pattern in a given location switches from one type to another over long time-scales.

Examples of weekly and monthly incidence time-series for four diseases (measles, chickenpox, rubella and whooping cough) are shown in figure 1*a–d*. On time-scales greater than a few months, patterns are evident. Figure 1*e–h* shows the power spectral densities (PSDs, see Appendix A) derived from segments of each of these time-series (Priestley 1981; Anderson *et al.* 1984). Peaks in the PSD identify the most prominent frequencies (f) and correspond to interepidemic intervals ($T = 1/f$) in the time-series. There are typically two distinct spectral peaks. The PSD almost always shows a peak corresponding to a period that is an integer multiple of 1 year (usually 1 or 2 years); we call this the *resonant peak*, as opposed to the *non-resonant peak*, which can apparently occur at any frequency. For a given disease, the positions of these peaks vary from place to place and, in a given place, over long time-scales.

The purpose of this paper is to explain the incidence patterns of these diseases using a mathematical model (described in § 2). Identification of the periods of the attractors of the model (which we term asymptotic analysis) correctly predicts the resonant PSD peaks but fails to predict the non-resonant peaks. We show that transient dynamics are the source of the non-resonant peaks and that these peaks can be predicted by a perturbation analysis of the model. Furthermore, we find that the relative magnitude of these two types of spectral peak is determined primarily by the degree of demographic stochasticity.

2. SEIR MODEL

The model is a seasonally forced version of the standard deterministic compartmental model known as the SEIR model (Anderson & May 1991). It divides the population into four compartments (S = susceptible, E = exposed but not yet infectious, I = infectious, R = recovered and immune). Rates of change of compartment size are given by ordinary differential equations:

$$\begin{aligned}\dot{S} &= \nu - (\beta I + \mu)S,\\ \dot{E} &= \beta IS - (\sigma + \mu)E,\\ \dot{I} &= \sigma E - (\gamma + \mu)I,\\ \dot{R} &= \gamma I - \mu R,\end{aligned} \tag{2.1}$$

where ν is the birth rate, μ is the *per capita* death rate, β is the mean transmission rate, $1/\sigma$ is the mean latent period and $1/\gamma$ is the mean infectious period. Seasonally varying transmission rates are specified according to school-term dates, with β high when school is in session and low otherwise (Schenzle 1984; Earn *et al.* 2000) (see Appendix B). The time-averaged mean transmission rate is denoted by $\langle\beta\rangle$. The amplitude of oscillation of β (relative to $\langle\beta\rangle$) can be approximated from transmission-rate reconstructions (Fine & Clarkson 1982; Finkenstadt & Grenfell 2000; see Appendix B).

3. ASYMPTOTIC ANALYSIS

A critical ingredient in the analysis of the model is an easily derived equivalence between changes in the mean transmission rate $\langle\beta\rangle$, the birth rate ν and the proportion of individuals vaccinated, p (fewer births or more vaccinations correspond to lower $\langle\beta\rangle$). If the birth rate changes from ν to ν' and/or if vaccination is initiated at coverage level p then the equivalent change in the mean transmission rate is given by (Earn *et al.* 2000):

$$\langle\beta\rangle \rightarrow \langle\beta\rangle\frac{\nu'}{\nu}(1 - p). \tag{3.1}$$

*Author for correspondence (bauch@math.mcmaster.ca).

© 2003 The Royal Society

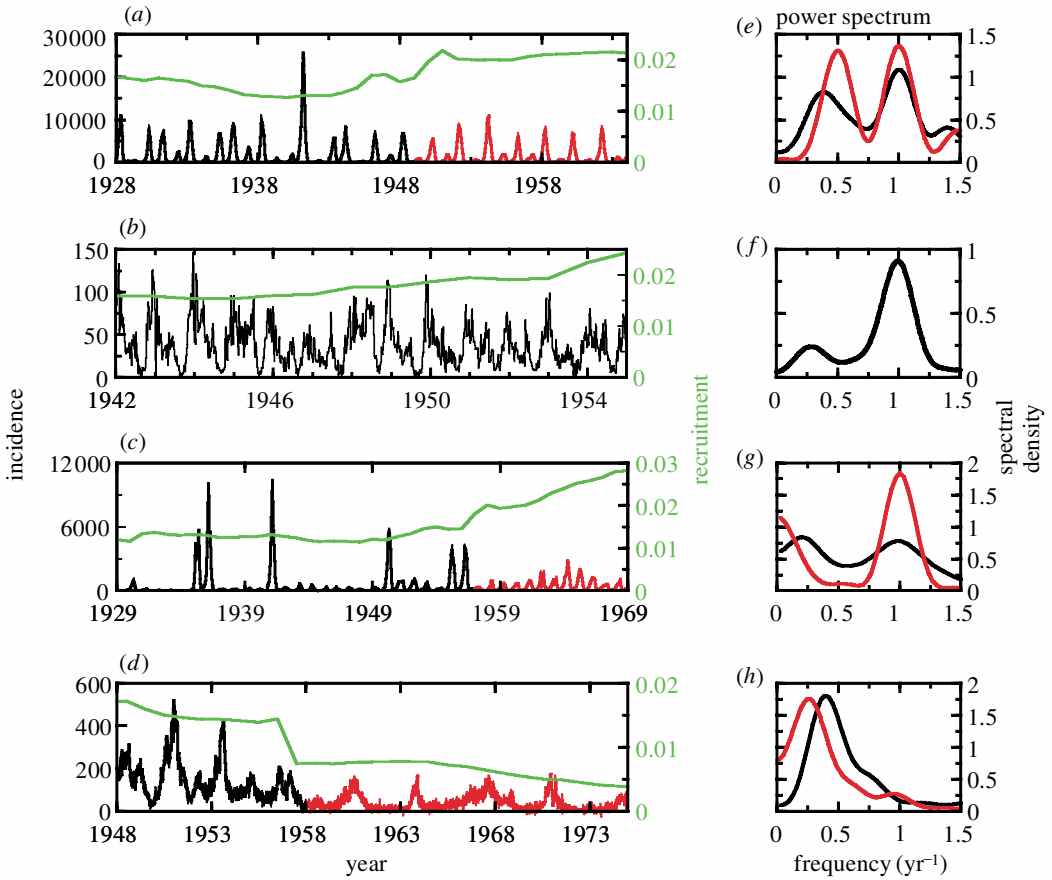

Figure 1. Examples of incidence time-series (*a–d*) and PSDs (*e–h*) for four childhood diseases. (*a*,*e*) Measles (New York City, USA); (*b*,*f*) chickenpox (Manitoba, Canada); (*c*,*g*) rubella (Ontario, Canada); and (*d*,*h*) whooping cough (London, UK). In each panel, the green line shows annual susceptible recruitment, $\nu(1-p)$, where ν denotes births normalized by 1955 population size and p denotes the proportion vaccinated (cf. Earn *et al.* 2000); recruitment is shown displaced forward in time by the mean age at infection to account for the typical delay between birth and infection (4 years for measles, 7 years for chickenpox, 11 years for rubella and 4 years for whooping cough). Time-series are divided into sections based on substantial differences in recruitment rates; the corresponding PSDs are not sensitive to the precise point at which the time-series is divided (the chickenpox time-series has not been divided because no dramatic change in births occurred during the period covered by the data). Wavelet analysis (Torrence & Compo 1998; Grenfell *et al.* 2001), which yields a PSD at each point in time, reveals similar spectral patterns. See Appendix A for details on the calculation of PSDs.

This equivalence makes it possible to predict major transitions in epidemic patterns from a bifurcation diagram showing the asymptotically stable solutions (i.e. the attractors) of the model as a function of $\langle\beta\rangle$. If a single attractor exists, this analysis predicts a simple cycle that yields a resonant peak in the PSD. If there are multiple attractors with densely intermixed basins then demographic stochasticity is predicted to cause the system to jump from one basin to another (Schwartz 1985; Earn *et al.* 2000). For cities for which birth and vaccination time-series are available, this asymptotic analysis of the model correctly predicts transitions in the patterns of measles epidemics (Earn *et al.* 2000), including changes in the resonant peaks of the PSD for measles incidence (e.g. figure 1*a*,*e*).

Applying this approach to chickenpox, we find that the model always shows several coexisting attractors. However, in the presence of noise, switching between attractors is infrequent and most time is spent in the basin of the annual attractor (see Appendix C). We can therefore understand the chickenpox time-series in figure 1*b* in terms of a system locked onto the annual attractor for a long time. Eventually, there might be a transition to a 3-year or 4-year cycle, but the timing of this transition is impossible to predict precisely. (Note that the traditional unforced SEIR model (Anderson & May 1991) incorrectly predicts that chickenpox should have an interepidemic interval of 3–4 years.)

The major features of the incidence patterns of rubella and whooping cough cannot be explained in terms of attractors. For both these diseases, the asymptotic analysis always predicts a single strictly annual cycle and hence a PSD peak at 1 year. In practice, a dominant non-resonant peak at a long period (2–6 years) is typically observed for these diseases (see figure 1*c*,*d*,*g*,*h*).

Previous work has suggested that this apparent failure of the model is related to stochasticity (Hethcote 1998; Rohani *et al.* 1999). Rohani *et al.* (1999) have shown that an event-driven Monte Carlo formulation of the model for whooping cough does produce a time-series with a non-annual spectral peak. However, the associated period is evident in simulations of the deterministic whooping cough model as trajectories approach the annual attractor (Keeling *et al.* 2000; Rohani *et al.* 2002).

For all the diseases we are examining here, we now show that the position of the non-resonant PSD peak is

not only predicted by the deterministic model and observed because of the presence of noise, but can also be calculated using a linear perturbation technique.

4. PERTURBATION ANALYSIS

The key new component of our analysis involves the application of linear perturbation theory to the attractors of the seasonally forced SEIR model. The solutions that we must perturb are the attractors, which, at their simplest, are annual cycles. Perturbation analysis of cyclical solutions of differential equations is a non-trivial problem, but a standard technique allows us to reduce it to analysis of fixed points (Kuznetsov 1998). In this way, we obtain the damping rate r_n and the oscillation period T_n of solutions that approach attractors corresponding to n-year epidemic cycles.

Rather than dealing with the full seasonally forced SEIR model directly, we derive its associated Poincaré map, which is equivalent to strobing the full system once a year. An annual cycle of the full system becomes a fixed point of the Poincaré map; a biennial cycle becomes a two-point cycle, etc. Since n-point cycles of the map are fixed points of the map composed with itself n times, linear analysis of all cycles reduces to that of fixed points. We do not have an analytical formula for the Poincaré map, so the linear analysis must, unfortunately, be carried out numerically; this is a nuisance, but standard methods (Kuznetsov 1998) yield precise results. For any n-point cycle of the Poincaré map, the stability analysis yields three eigenvalues that determine the transient dynamics near the associated periodic cycle of the full system. Because the latent and infectious periods of childhood diseases are much shorter than a typical human lifetime, one eigenvalue has a small modulus, causing rapid collapse of the solutions onto a centre manifold (Schwartz & Smith 1983). The remaining two eigenvalues are complex conjugates and hence have the same modulus $|\lambda_n|$ and magnitude of argument $|\mathrm{Arg}(\lambda_n)|$. In the case of a stable cycle, solutions undergo damped oscillations onto the n-point attractor with a damping rate

$$r_n \equiv \ln\frac{1}{|\lambda_n|},$$

and an oscillation period

$$T_n \equiv \frac{2\pi n}{|\mathrm{Arg}(\lambda_n)|}.$$

5. STOCHASTIC EFFECTS

As pointed out by Bartlett in relation to unforced epidemic models (Bartlett 1957), demographic stochasticity can sustain oscillations that would be damped out in the absence of noise. The same mechanism applies to the seasonally forced model we are examining here. Noise can prevent oscillations at period T_n from damping out, leading to a non-resonant peak at period T_n in the PSD. Although noise inhibits convergence onto the attractor, r_n provides a measure of the sensitivity of the attractor to noise and the population size N determines the degree of demographic stochasticity. Note that we call the periods T_n *non-resonant* because they are stimulated by demographic stochasticity, in contrast to the *resonant* periods, which are associated with the attractors themselves (and resonate with the seasonal forcing period of 1 year).

While the asymptotic analysis predicts the period of the resonant PSD peak, and the perturbation analysis reveals the period of the non-resonant PSD peak, neither analysis determines how large each of these peaks should be. To explain fully the observed PSDs we must find a way to predict the relative magnitude of the resonant and non-resonant peaks. The ratio of peak magnitudes determines the relative importance of seasonality versus demographic stochasticity, i.e. the relative importance of asymptotic cycles versus transient (noise-sustained) effects.

To discover which factors influence the relative magnitude of non-resonant and resonant peaks we analysed simulations of the event-driven Monte Carlo formulation (Bartlett 1957) of the seasonally forced SEIR model. This analysis showed that the relative magnitude of the PSD peaks is sensitive to the mean transmission rate $\langle\beta\rangle$, the amplitude of seasonal forcing α and the population size N. The ratio of non-resonant to resonant peaks decreases with increasing $\langle\beta\rangle$, increasing α and, as expected, increasing N.

6. COMBINED ANALYSIS

To predict the character of an incidence time-series (including transitions induced by changes in birth rate and vaccination levels) from estimates of disease and demographic parameters, we must carry out a combined analysis involving the three procedures we have discussed in §§ 3–5 (asymptotic analysis, perturbation analysis and relative peak-magnitude analysis).

Figure 2 shows an example of this combined analysis for the case of whooping cough. Each panel shows an aspect of the dynamics predicted as a function of $\langle\beta\rangle$. Figure 2*a* shows the bifurcation diagram of the attractors: for whooping cough there is a simple annual cycle for all $\langle\beta\rangle$, so a resonant peak in the PSD at 1 year is always predicted. For measles (Earn *et al.* 2000), chickenpox and rubella, the bifurcation diagram would also display biennial, triennial and other multiennial attractors for certain ranges of $\langle\beta\rangle$ (though, as mentioned in § 3, stochastic simulations spend most time in the vicinity of the 1-year and 2-year attractors).

Figure 2*b* shows the transient period T_1 as a function of $\langle\beta\rangle$. T_1 predicts the position of the non-resonant PSD peak. We do not need to consider T_n for $n \geqslant 2$, because in such cases the transient period is longer than the sections of the time-series for which birth rates and vaccine uptake remain approximately constant; hence the transient period is unobservable in these cases. This is true for all the diseases we are considering here. (One easily verifiable prediction resulting from this is that there should be no non-resonant peak in the measles time-series when the system is in the regime with a unique biennial attractor.) Therefore, even when multiple attractors coexist, T_1 is the only non-resonant period that we expect to appear as a PSD peak.

Finally, figure 2*c* shows the ratio of the magnitude of the non-resonant peak to the magnitude of the resonant peak as a function of $\langle\beta\rangle$, for several population sizes relevant to the whooping cough data we are considering here.

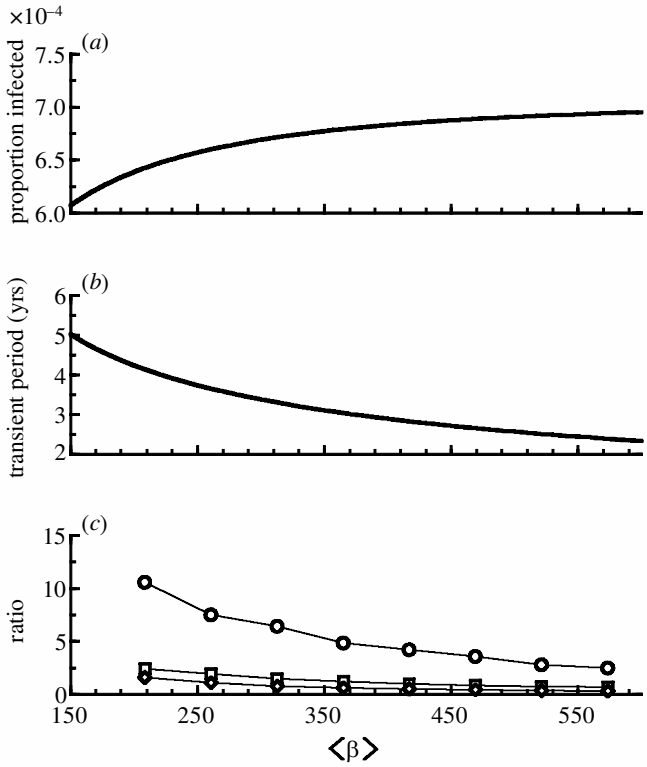

Figure 2. Three-part 'transition diagram' for whooping cough. Changes in the resonant period are predicted by (*a*), which shows the attractors that are present as a function of $\langle\beta\rangle$ (for whooping cough an annual cycle is predicted for all $\langle\beta\rangle$). Likewise, changes in the transient (non-resonant) period T_1 are predicted by (*b*), and changes in the ratio of the magnitudes of non-resonant to resonant peaks are predicted by (*c*), which shows results from stochastic simulations (circles: $N = 1$ million; squares: $N = 4$ million; diamonds: $N = 8$ million). The disease parameters are mean latent period $1/\sigma = 14$ days and mean infectious period $1/\gamma = 8$ days. The seasonal amplitude is $\alpha = 0.15$.

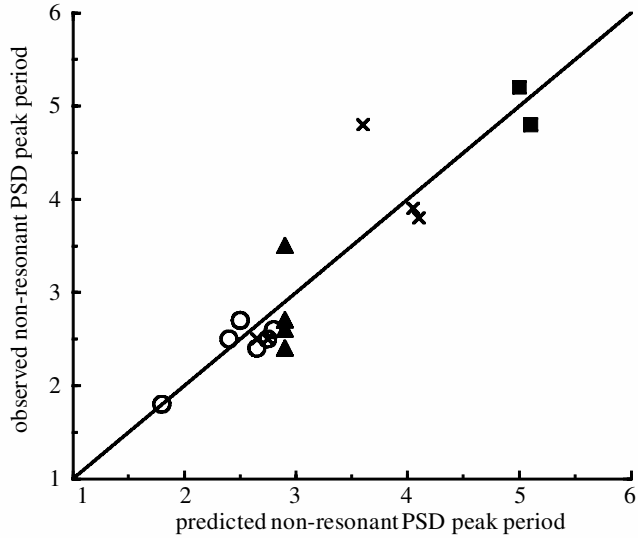

Figure 3. The correlation between predicted and observed periods of non-resonant PSD peaks is positive and highly significant ($r^2 = 0.83$, $t = 8.69$, d.f. = 16, $p < 10^{-7}$). If the observations agreed perfectly with our predictions (as they do for resonant PSD peaks) then the corresponding points would lie precisely on the line of slope 1 shown on the graph (the least-squares linear fit of the data has a slope of 1.02 and an intercept of −0.11). Circles, measles; triangles, chickenpox; squares, rubella; crosses, whooping cough. See electronic Appendix A for parameter estimates and for the results in tabular format.

The damping rate r_1, which controls the rate of convergence to the attractor, increases monotonically with $\langle\beta\rangle$, hence we can display the results of the perturbation analysis as a function of $\langle\beta\rangle$, just as we can with the asymptotic analysis; Earn *et al.* (2000). Furthermore, the amplitude α is a fixed parameter for a given disease in a given place and does not vary significantly even between places (see electronic Appendix A; available on The Royal Society's Publications Web site). Consequently, for predicting the relative magnitude we need worry only about changes in the effective $\langle\beta\rangle$ resulting from birth rate and vaccination changes and differences in population size N between different places.

Three-part 'transition diagrams' such as figure 2 allow us to predict the character of an infectious disease time-series and how it will change in response to changes in birth rate or vaccination level. For a given place, an estimate of the basic reproductive ratio $\mathscr{R}_0$ (Anderson & May 1991) at a given time allows us to compute $\langle\beta\rangle$ at that time and hence to predict the PSD peak locations from figure 2*a*,*b* and their relative magnitude from figure 2*c*. If the birth rate changes from ν to ν' and vaccination of a proportion p of infants is initiated then the predicted transition in PSD peaks and relative magnitude can be determined from these diagrams by the equivalence given in equation (3.1).

7. RESULTS AND DISCUSSION

We applied this combined analysis to all childhood disease time-series for which disease incidence, birth rates and vaccine uptake data were available to us. In the asymptotic analysis (as in figure 2*a*), the resonant PSD peak in each time-series is perfectly predicted (see table 1 of electronic Appendix A). In the perturbation analysis (as in figure 2*b*), the observed positions of the non-resonant peaks are strongly correlated with those predicted (see figure 3). These results vindicate the seasonally forced SEIR model for all four diseases. (They also supplement previous work on measles (Earn *et al.* 2000), since both non-resonant and resonant peaks are predicted; it so happens that the main features of measles dynamics are usually described by resonant peaks in the PSD, which is why perturbation analysis was not required to predict transitions in the major features.)

We are not able to predict the precise ratio of the magnitudes of peaks in the real incidence data, and with good reason. Our stochastic simulations show that spectra of short segments (e.g. 50 years) of a given disease time-series can have very different ratios of peak magnitudes (e.g. varying from 0.5 to 2 in the case of whooping cough). Nevertheless, the directions of change in the peak ratio as $\langle\beta\rangle$ or N change can be robustly predicted: diseases with higher effective $\mathscr{R}_0$ and greater seasonal forcing (α) will have more power in the resonant PSD peak; moreover, for a given disease, smaller populations (which yield greater demographic stochasticity) will have more power in the

non-resonant peak. These general relationships are seen, for example, in whooping cough power spectra for British cities in the twentieth century before, and after, mass vaccination was initiated (Rohani *et al.* 2000) and in the rubella and chickenpox data that we have analysed here (see figures 1*b*,*c*,*f*,*g* and 3, and table 1 of electronic appendix A). Furthermore, it has previously been noted that smaller towns typically exhibit multiennial outbreaks of chickenpox whereas large cities always exhibit annual outbreaks (Olsen *et al.* 1988). Diseases such as measles and chickenpox, with moderate to large values of $\mathscr{R}_0$ and α, typically exhibit large resonant power, whereas diseases such as whooping cough (which has a small α) and rubella (which has a small $\mathscr{R}_0$) exhibit significant non-resonant power.

This success suggests that there is every reason to expect that analyses like these will be extremely useful for predicting patterns of epidemics of other diseases and, more generally, the population dynamics of other ecological systems.

Recent work has shown that transient dynamics may dominate ecological dynamics and that restricting attention to attractors of models may miss the most important dynamic features of ecological systems (Hastings & Higgins 1994). Our analysis supports this view, but at the same time highlights the importance of studying the attractors, since a stability analysis of those states can reveal the nature of observed noise-sustained transients in real ecological systems.

The authors thank David Rand and Nigel Burroughs for helpful discussions, and Jonathan Dushoff, Alison Galvani, Rufus Johnstone and Pej Rohani for comments on an early version of the manuscript. D.J.D.E. is supported by the Natural Sciences and Engineering Research Council of Canada (NSERC), the Canadian Institutes for Health Research (CIHR), the Canada Foundation for Innovation (CFI) and an Ontario Premier's Research Excellence Award. Computer simulations were performed on Sharcnet (www.sharcnet.ca).

APPENDIX A: POWER SPECTRAL DENSITY CALCULATION

The PSD is the Fourier transform of the autocovariance function of the time-series (Priestley 1981; Anderson *et al.* 1984). Before computation of the PSD the data were trend-corrected and tapered with a double cosine bell (Priestley 1981). The autocovariance function was smoothed with a Tukey window (Priestley 1981) to reduce the variance in the PSD, which facilitates location of the PSD peaks. The width of the Tukey window was chosen so that the resulting bandwidth was the same (0.35) for both weekly and monthly incidence time-series.

APPENDIX B: SEASONAL FORCING

We introduce seasonal variation in contact rates into the SEIR model (equation (2.1)) by replacing the constant parameter β with a time-varying function $\beta(t)$ that is high on days when school is in session and low otherwise:

$$\beta(t) = \begin{cases} \beta_{\mathrm{H}} \text{ on school days,} \\ \beta_{\mathrm{L}} \text{ on non-school days.} \end{cases} \tag{B 1}$$

If the proportion of days in school is s then the time-averaged mean transmission rate is:

$$\langle\beta\rangle = s\beta_{\mathrm{H}} + (1-s)\beta_{\mathrm{L}} \tag{B 2}$$

and we define the amplitude of seasonality to be:

$$\alpha = \frac{1}{2}\left(\frac{\beta_{\mathrm{H}} - \beta_{\mathrm{L}}}{\langle\beta\rangle}\right). \tag{B 3}$$

In terms of $\langle\beta\rangle$ and α we can write the transmission rate as:

$$\beta(t) = \begin{cases} [(1 + 2(1 - s)\alpha]\langle\beta\rangle \text{ on school days,} \\ [1 - 2s\alpha]\langle\beta\rangle \text{ on non-school days.} \end{cases} \tag{B 4}$$

Note that, since $\beta(t) \geqslant 0$, it is clear from equation (B 4) that the range over which the seasonal amplitude α can be varied is

$$0 \leqslant \alpha \leqslant \frac{1}{2s}. \tag{B 5}$$

At the maximum amplitude $\beta_{\mathrm{L}} = 0$, i.e. $\beta(t) = 0$ on non-school days.

As a parameter of the model, the amplitude of seasonality α is unique in that it must be estimated from the incidence time-series. All other parameters, including $\langle\beta\rangle$, are estimated independently of the incidence time-series. We used a standard method (Fine & Clarkson 1982) to reconstruct the seasonally varying transmission rate from the incidence record (we call this reconstructed transmission rate $\beta_{\mathrm{rec}}(t)$), and then estimated α by insisting that the area bounded by the imposed seasonality function (about its mean) is identical to the area bounded by the reconstructed seasonality function (about its mean). More precisely, we set

$$\int_0^1 \left|\frac{\beta_{\mathrm{rec}}(t)}{\langle\beta_{\mathrm{rec}}\rangle} - 1\right| \mathrm{d}t = \int_0^1 \left|\frac{\beta(t)}{\langle\beta\rangle} - 1\right| \mathrm{d}t, \tag{B 6}$$

where $\beta(t)$ is given by equation (B 4), and $\langle\beta_{\mathrm{rec}}\rangle$ denotes the time average of $\beta_{\mathrm{rec}}(t)$. Solving equation (B 6) for α yields

$$\alpha = \frac{1}{4(s - s^2)} \int_0^1 \left|\frac{\beta_{\mathrm{rec}}(t)}{\langle\beta_{\mathrm{rec}}\rangle} - 1\right| \mathrm{d}t. \tag{B 7}$$

See table 3 in electronic Appendix A for the resulting estimates of α. This method of estimating the seasonal amplitude is justified by the fact that the dynamic structure of the model (i.e. its bifurcation diagram) is almost identical when the seasonal forcing function is transformed keeping the total area it bounds constant (D. J. D. Earn and C. T. Bauch, unpublished data).

Simulations of the stochastic formulation of the model show that the estimate of α given by equation (B 7) is not sensitive to the degree of demographic stochasticity (i.e. population size N) or to the proportion of the population that is vaccinated (p). Thus, there is no reason to segment the time-series when using this technique to estimate the seasonal amplitude. Accordingly, the estimates of α given in electronic Appendix A were obtained by applying equation (B 7) to the longest weekly time-series available for each location.

APPENDIX C: SWITCHING BETWEEN ATTRACTORS

The stochastic simulations reveal how demographic stochasticity causes switching between the basins of differ-

ent attractors. For chickenpox, multiple attractors are always present. For measles, multiple attractors are present when transmission rates are low (so the effective $\mathcal{R}_0 \leqslant 15$; for example, New York City before the Second World War). In both cases, jumps between basins typically occur on time-scales much longer than the empirical time-series (e.g. less often than once per century), and the stochastic simulations spend almost all of their time in the basin of the annual attractor; hence a unique resonant peak at 1 year should usually occur in these cases.

REFERENCES

Anderson, R. M. & May, R. M. 1991 *Infectious diseases of humans*. Oxford University Press.

Anderson, R. M., Grenfell, B. T. & May, R. M. 1984 Oscillatory fluctuations in the incidence of infectious disease and the impact of vaccination: time series analysis. *J. Hyg. Camb.* **93**, 587–608.

Bartlett, M. S. 1957 Measles periodicity and community size. *J. R. Statist. Soc.* **120**, 48–70.

Bolker, B. M. & Grenfell, B. T. 1993 Chaos and biological complexity in measles dynamics. *Proc. R. Soc. Lond.* B **251**, 75–81.

Dietz, K. 1975 Transmission and control of arbovirus diseases. In *Epidemiology* (ed. D. Ludwig & K. L. Cooke), pp. 104–121. Philadelphia, PA: SIAM.

Earn, D. J. D., Rohani, P. & Grenfell, B. T. 1998 Persistence, chaos and synchrony in ecology and epidemiology. *Proc. R. Soc. Lond.* B **265**, 7–10. (DOI 10.1098/rspb.1998.0256.)

Earn, D. J. D., Rohani, P., Bolker, B. M. & Grenfell, B. T. 2000 A simple model for complex dynamical transitions in epidemics. *Science* **287**, 667–670.

Fine, P. E. M. & Clarkson, J. A. 1982 Measles in England and Wales. I. An analysis of factors underlying seasonal patterns. *Int. J. Epidemiol.* **11**, 5–14.

Finkenstadt, B. & Grenfell, B. T. 2000 Time series modelling of childhood infectious diseases: a dynamical systems approach. *J. R. Statist. Soc.* C **49**, 187–205.

Grenfell, B. T. 1992 Chance and chaos in measles dynamics. *J. R. Statist. Soc.* B **54**, 383–398.

Grenfell, B. T., Bjornstad, O. N. & Kappey, J. 2001 Travelling waves and spatial hierarchies in measles epidemics. *Nature* **414**, 716–723.

Hastings, A. & Higgins, K. 1994 Persistence of transients in spatially structured ecological models. *Science* **263**, 1133–1136.

Hethcote, H. W. 1998 Oscillations in an endemic model for pertussis. *Can. Appl. Math. Q.* **6**, 61–88.

Keeling, M. J., Rohani, P. & Grenfell, B. T. 2000 Seasonally forced disease dynamics explored as switching between attractors. *Physica* D **148**, 317–335.

Kuznetsov, Y. A. 1998 *Elements of applied bifurcation theory*. New York: Springer.

London, W. & Yorke, J. A. 1973 Recurrent outbreaks of measles, chickenpox and mumps. I. Seasonal variation in contact rates. *Am. J. Epidemiol.* **98**, 469–482.

Olsen, L. F. & Schaffer, W. M. 1990 Chaos versus noisy periodicity: alternative hypothesis for childhood epidemics. *Science* **249**, 499–504.

Olsen, L. F., Truty, G. L. & Schaffer, W. M. 1988 Oscillations and chaos in epidemics: a nonlinear dynamic study of six childhood diseases in Copenhagen, Denmark. *Theor. Popul. Biol.* **33**, 344–370.

Priestley, M. B. 1981 *Spectral analysis and time series*. London: Academic Press.

Rohani, P., Earn, D. J. D. & Grenfell, B. T. 1999 Opposite patterns of synchrony in sympatric disease metapopulations. *Science* **286**, 968–971.

Rohani, P., Earn, D. J. D. & Grenfell, B. T. 2000 The impact of immunisation on pertussis transmission in England and Wales. *Lancet* **355**, 285–286.

Rohani, P., Keeling, M. J. & Grenfell, B. T. 2002 The interplay between determinism and stochasticity in childhood diseases. *Am. Nat.* **159**, 469–481.

Schaffer, W. M. 1985 Can nonlinear dynamics elucidate mechanisms in ecology and epidemiology? *IMA J. Math. Appl. Med. Biol.* **2**, 221–252.

Schenzle, D. 1984 An age-structure model of pre- and post-vaccination measles transmission. *IMA J. Math. Appl. Med. Biol.* **1**, 169–191.

Schwartz, I. B. 1985 Multiple stable recurrent outbreaks and predictability in seasonally forced nonlinear epidemic models. *J. Math. Biol.* **21**, 347–361.

Schwartz, I. B. & Smith, H. L. 1983 Infinite subharmonic bifurcation in an SEIR epidemic model. *J. Math. Biol.* **18**, 233–253.

Torrence, C. & Compo, G. P. 1998 A practical guide to wavelet analysis. *Bull. Am. Meteorol. Soc.* **79**, 61–78.

Yorke, J. A. & London, W. 1973 Recurrent outbreaks of measles, chickenpox and mumps. II. Systematic differences in contact rates and stochastic effects. *Am. J. Epidemiol.* **98**, 453–468.

Visit http://www.pubs.royalsoc.ac.uk to see an electronic appendix to this paper.

This is an electronic appendix to the paper by Bauch & Earn 2003 Transients and attractors in epidemics. *Proc. R.. Soc. Lond.* B **270**, 1573-1578. (DOI 10.1098/rspb.2003.2410.)

Electronic appendices are refereed with the text. However, no attempt has been made to impose a uniform editorial style on the electronic appendices.

Tabulated Results

Table 1 shows the predicted and observed resonant and non-resonant periods for all the incidence time series we have studied.

As in the examples in Figure 1, all time series were broken into sections of roughly constant recruitment rate. This sectioning of the time series is important because substantial differences in recruitment rates yield different predictions for the PSD peaks, i.e., dynamical transitions are induced by substantial changes in recruitment rates (Earn *et al.* 2000).

In Table 1, a superscript 'b' indicates that a major change in recruitment rate was caused by a change in the number of births, while a superscript 'v' indicates that the proportion vaccinated changed substantially (either mass vaccination was initiated or a vaccine scare led to a dramatic reduction in vaccine uptake).

A large boost in births occurred during the 'baby boom' following the Second World War. The effects of birth rate changes on transmission dynamics are delayed, approximately, by the mean age at infection, A. Therefore, before calculating recruitment rates, $\nu(1-p)$, we translated the birth time series forward by A (4 years for measles, 7 years for chicken pox, 11 years for rubella and 4 years for whooping cough; *cf.* caption to Figure 1). Note that A will, of course, decrease (increase) as larger (smaller) birth cohorts age; however, correcting for this would lead only to a small difference in the amount by which the birth time series is translated forward.

In contrast, the effects of vaccination are almost immediate because — at least during the periods that the data cover — vaccine was administered primarily to children who were already experiencing high contact rates. In the case of whooping cough in London, England, whole cell vaccination was introduced in 1957, but there was a sharp decrease

in uptake in 1974 due to a vaccine scare. Vaccination against rubella was introduced in Canada in 1969, and vaccination against measles in England and Wales was started in 1967.

For vaccine era measles in London and Liverpool, England, and for whooping cough in London from 1978 onwards, the non-resonant period increased as vaccine uptake gradually increased; this is the reason for the ranges given in the table. To obtain the PSD peak range from these time series, we used a wavelet analysis (Torrence & Compo 1998, Grenfell *et al.* 2001). The midpoint period of the range is plotted in Figure 3 in these cases.

Parameter Estimates

Tables 2, 3 and 4 show the estimated parameter values that we used to obtain predictions for the resonant and non-resonant PSD peaks in all the incidence time series. Below, when we refer to published parameter estimates, they were taken from the monograph of Anderson & May (1991) and from standard vital statistics publications.

The mean latent period ($1/\sigma$) and mean infectious period ($1/\gamma$) for each disease are given in Table 2. Table 3 shows estimates of α, and Table 4 shows estimates of R_0 and $\langle\beta\rangle$.

Empirical estimates of the basic reproductive ratio R_0 yield $\langle\beta\rangle$ according to the relation $\langle\beta\rangle \simeq \gamma R_0$ (Anderson & May 1991). When available, we used published estimates of R_0 based on age-structured serological and incidence data, relevant either to the same place and time under analysis, or for a similar place and time. For other places and times it was necessary to estimate an effective R_0; we did this by starting with a known estimate of R_0 for another place or time, and then taking into account differences in birth rates and/or vaccine coverage (*cf.* Eq. 3.1 and Earn *et al.* (2000)). Whenever Eq. 3.1 was used in estimating the *effective* basic reproductive ratio, $R_{0,\mathrm{eff}}$, we flagged the corresponding entry in Table 4 with a superscript '*'.

For measles in London, England (1950–1967), New York City (1951–1963) and Baltimore (1951–1959) we used a published estimate of $R_0 \approx 17$ based on age-structured data for England and Wales (1950–1958). Then, inserting published birth records into Eq. 3.1, we estimated $R_{0,\mathrm{eff}}$ for the years before the baby boom in these locations. For

measles in Ontario (1904–1948) we again used a published estimate of $R_0 \approx 10.5$, based on age-structured data for Ontario (1912–1913).

For chicken pox in the Canadian provinces (1942–1955) and New York City (1928–1955), we used the estimate $R_0 \approx 10.5$ for chicken pox in Baltimore in 1943.

For rubella, the published estimate is $R_0 \approx 6.5$ for England and Wales (1960–1970). It would not be unreasonable to adopt this value for R_0 in Ontario during the same time period. Unfortunately, we are unable to use Eq. 3.1 to estimate the $R_{0,\text{eff}}$ after mass vaccination was initiated, because we have no data on rubella vaccine uptake levels in Ontario. Instead, we have adopted a method for estimating $R_{0,\text{eff}}$ for rubella in Ontario that can be carried out for each of the three sections in the time series available to us. We used the approximation $R_0 \simeq G/A$, where G is the inverse of the per capita birth rate and A is the mean age at infection, which is derived in Anderson & May (1991). We estimated G from Ontario birth and population data for each of the three sections of the rubella time series. Since we do not have age-structured rubella data, we used published values for the mean age at infection for the relevant time periods in the USA (See Table 5.4 in Anderson & May (1991)). The mean age at infection by rubella in the USA (1978–1980) was $A_{\text{USA}} \approx$ 13–16 years, so we took $A = 14.5$ years for Ontario (1970–1989) ($G = 69.9$). $A_{\text{USA}} \approx 9.5$ for the USA (1966–1968), so we took $A = 9.5$ for Ontario (1957–1969) ($G = 55.4$). $A_{\text{USA}} \approx 10.5$ in 1943, so we took $A = 0.5$ for Ontario (1929–1956) ($G = 48.3$).

Finally, for whooping cough, the published England and Wales (1944–1978) estimate of $R_0 \approx 17$ was used as the R_0 for London, England (1958–1974). The value for London (1978–1991) was computed using Eq. 3.1 and taking changes in birth rates and vaccine coverage into account. For whooping cough in London, vaccination was initiated in 1957 but we were able to obtain yearly vaccine uptake data only from 1966 (Miller & Gay 1997); following Rohani *et al.* (1999), we interpolated vaccine uptake from 60% in 1958 to 75% in 1966 with vaccine efficacy of 80%. The published estimate $R_0 \approx$ 10–11 for Ontario (1912–1913) was used for Ontario (1904–1913), and Eq. 3.1 supplied us with an estimate for Ontario (1925–1943).

References

Anderson, R. M. & May, R. M. 1991, *Infectious Diseases of Humans*, Oxford Univ. Press, Oxford.

Earn, D. J. D., Rohani, P., Bolker, B. M. & Grenfell, B. T. 2000, A simple model for complex dynamical transitions in epidemics, *Science* **287**, 667–670.

Grenfell, B. T., Bjornstad, O. N. & Kappey, J. 2001, Travelling waves and spatial hierarchies in measles epidemics, *Nature* **414**, 716–723.

Miller, E. & Gay, N. J. 1997, Epidemiological determinants of pertussis, *Dev. Biol. Stand.* **89**, 15–23.

Rohani, P., Earn, D. J. D. & Grenfell, B. T. 1999, Opposite patterns of synchrony in sympatric disease metapopulations, *Science* **286**, 968–971.

Torrence, C. & Compo, G. P. 1998, A practical guide to wavelet analysis, *Bull. Amer. Meteor. Soc.* **79**, 61–78.

Disease	Place & Time	Predicted Spectral Peak (yrs)		Observed Spectral Peak (yrs)	
		Nonres.	Res.	Nonres.	Res.
Measles	London, England 1950–1967^{v}	–	2	–	2
	London, England 1968^{v}–1988	2.0–3.5	1	2.0–3	1
	Liverpool, England 1944–1967^{v}	1.8	1	1.8	1
	Liverpool, England 1968^{v}–1988	1.8–3.5	1	1.8–3	1
	Ontario, Canada 1904–1948	2.5	1	2.7	1
	NYC, USA 1928–1950^{b}	2.4	1	2.5	1
	NYC, USA 1951^{b}–1963	–	2	–	2
	Baltimore, USA 1928–1950^{b}	2.8	1	2.6	1
	Baltimore, USA 1951^{b}–1959	–	2	–	2
Chicken Pox	Ontario, Canada 1942–1955	2.9	1	2.7	1
	Manitoba, Canada 1942–1955	2.9	1	3.5	1
	BC, Canada 1942–1955	2.9	1	2.4	1
	Sasketchewan, Canada 1942–1955	2.9	1	2.6	1
	NYC, USA 1928–1955	2.9	1	–	1
Rubella	Ontario, Canada 1929–1956^{b}	5.1	1	4.8	1
	Ontario, Canada 1957^{b}–1969^{v}	4.1	1	–	1
	Ontario, Canada 1970^{v}–1989	5.0	1	5.2	1
Whooping Cough	London, England 1948–1957^{v}	2.7	1	2.5	–
	London, England 1958^{v}–1974^{v}	4.1	1	3.8	1
	London, England 1978^{v}–1991	3.7–4.4	1	3.8–4	1
	Ontario, Canada 1904–1913	3.6	1	4.8	–
	Ontario, Canada 1925–1943	2.7	1	2.5	–

Table 1: Predicted and observed periods of non-resonant and resonant power spectral density (PSD) peaks. The model perfectly predicts all resonant PSD peaks. The correlation between predicted and observed non-resonant PSD peaks is shown in Figure 3. *'b'* denotes a transition induced by changes in birth rates and *'v'* denotes a transition induced by changes in vaccine uptake. Further details are given in the text.

Disease	$1/\sigma$ (days)	$1/\gamma$ (days)
Measles	8	5
Chicken Pox	10	5
Rubella	10	7
Whooping Cough	8	14

Table 2: Values of the mean latent period $1/\sigma$ and the mean infectious period $1/\gamma$ used in the analysis of the seasonally forced SEIR model. Source: Anderson & May (1991), Table 3.1.

Disease	Place & Time	α
Measles	London, England 1944–1988	0.20
	Liverpool, England 1944–1988	0.16
	Ontario, Canada 1939–1969	0.21
Chicken Pox	Ontario, Canada 1942–1955	0.22
	Manitoba, Canada 1942–1955	0.22
	BC, Canada 1942–1955	0.20
	Sasketchewan, Canada 1942–1955	0.22
Rubella	Ontario, Canada 1939–1989	0.21
Whooping Cough	London, England 1948–1991	0.10
	Ontario, Canada 1939–1969	0.14

Table 3: Estimates of the seasonal amplitude α, based on Eq. B7. For each disease in each location, the longest weekly incidence series available to us was used in Eq. B7. See Appendix B for a description of the estimation technique. Our estimates of α are consistent with more crude estimates of α reported previously (Earn *et al.* 2000, Rohani *et al.* 1999).

Disease	Place & Time	Data type	$R_{0,\mathrm{eff}}$	$\langle\beta\rangle$ (yr^{-1})
Measles	London, England 1950–1967	W	17	1241
	London, England 1968–1986	W	6.8*–17	496–1241
	Liverpool, England 1944–1967	W	25.6*	1869
	Liverpool, England 1968–1988	W	6.9*–25.6*	504–1869
	Ontario, Canada 1904–1948	M	11.5	840
	NYC, USA 1928–1950	M	12.2*	891
	NYC, USA 1951–1963	M	17	1241
	Baltimore, USA 1928–1950	M	9.9*	723
	Baltimore, USA 1951–1959	M	17	1241
Chicken Pox	Ontario, Canada 1942–1955	W	10.5	767
	Manitoba, Canada 1942–1955	W	10.5	767
	BC, Canada 1942–1955	W	10.5	767
	Sasketchewan, Canada 1942–1955	W	10.5	767
	NYC, USA 1928–1955	M	10.5	767
Rubella	Ontario, Canada 1929–1956	M	4.6	240
	Ontario, Canada 1957–1969	W	6.5	339
	Ontario, Canada 1970–1989	M	4.8	250
Whooping Cough	London, England 1948–1957	W	17	443
	London, England 1958–1974	W	8.0*	209
	London, England 1978–1991	W	7.2*–9.9*	188–258
	Ontario, Canada 1904–1913	M	10.5	274
	Ontario, Canada 1925–1943	M	17.3*	451

Table 4: Parameter values used in the analysis of the seasonally forced SEIR model. The 'Data type' indicates whether cases were reported weekly (W) or monthly (M). '*' indicates that an effective value of R_0 for a given place and time, $R_{0,\mathrm{eff}}$, was calculated based on an R_0 value from a different place or time, using Eq. 3.1 together with data on birth rates and vaccine uptake. Further details are given in the text.